

# New Liquid Chemical Hydrogen Storage Technology

Subjects: [Chemistry, Applied](#) | [Nanoscience & Nanotechnology](#) | [Chemistry, Physical](#)

Contributor: Xinchun Yang , Dmitri A. Bulushev , Jun Yang , Quan Zhang

The liquid chemical hydrogen storage technology has great potentials for high-density hydrogen storage and transportation at ambient temperature and pressure. However, its commercial applications highly rely on the high-performance heterogeneous dehydrogenation catalysts, owing to the dehydrogenation difficulty of chemical hydrogen storage materials. The chemists and materials scientists found that the supported metal nanoparticles (MNPs) can exhibit high catalytic activity, selectivity, and stability for the dehydrogenation of chemical hydrogen storage materials, which will clear the way for the commercial application of liquid chemical hydrogen storage technology.

hydrogen storage

formic acid

hydrazine hydrate

## 1. Introduction

Hydrogen is a clean, efficient, and renewable energy carrier towards driving a carbon neutral future <sup>[1][2]</sup>. The World's leading economies, including the United States, China, Japan, Russia, South Korea, and the European Union, have pumped a vast amount of money into commercializing the newly developed hydrogen energy technology. However, hydrogen is flammable, easy to diffuse, and difficult to store and transport, restricting its large-scale applications. Developing efficient, safe, and long-distance hydrogen storage systems is highly anticipated.

The current hydrogen storage systems mainly include <sup>[3][4]</sup> high-pressure gas cylinders, cryogenic liquid cylinders, metal hydrides, and porous materials (zeolite, activated carbon, metal-organic frameworks (MOFs), etc.). It is difficult for these systems to meet the requirements of the large-scale applications of hydrogen. For example, high-pressure gas/cryogenic liquid cylinders face problems such as high difficulty in cylinder manufacturing, high energy consumption in gas compression process, and hidden dangers during operation. Metal hydrides face problems such as high cost, high absorption/dehydrogenation temperature and low durability; while porous materials have low hydrogen storage density at room temperature.

In recent years, liquid chemical hydrogen storage technology has attracted much attention as a novel strategy for high-density hydrogen storage and transportation at ambient conditions <sup>[5][6]</sup>. Since liquid chemical compounds have similar features to the common fuels, such as diesel and gasoline, and their hydrogen is stored forming chemical bonds, high-density hydrogen can be transported, stored and refilled safely by using existing petroleum infrastructure. However, the dehydrogenation of liquid chemical hydrogen storage materials faces large challenges

owing to their thermodynamic and kinetic factors. A list of chemical hydrogen storage materials includes different classes of compounds. Among them ammonia borane, formic acid, alcohols, hydrazine hydrate, aromatic compounds, and N-heteroaromatic compounds should be mentioned [6].

Fortunately, the supported metal nanoparticles (MNPs) can exhibit an excellent catalytic performance in the hydrogen production from liquid chemical hydrogen storage materials, owing to their small size effect, synergistic effect, and metal–support interaction [7][8][9][10]. In addition, compared with homogeneous catalysts, the supported MNPs are easy to separate and recycle, providing a promising route to reducing the catalyst cost for commercial applications.

## 2. Formic Acid Dehydrogenation

Formic acid (HCOOH) is a promising liquid chemical hydrogen material owing to its advantages of low toxicity, high hydrogen content (4.4 wt.%), high stability, and easy availability through biomass processing and CO<sub>2</sub> hydrogenation [11][12][13]. The stored hydrogen in formic acid can be released through two pathways, dehydrogenation (1) and dehydration (2) [14]:



Given that dehydration (2) not only reduces hydrogen production but also generates carbon monoxide (which is toxic to dehydrogenation and fuel cell catalysts), the key to the practical application of formic acid dehydrogenation lies in the development of high-performance MNP catalysts. These catalysts can be used for gas-phase or liquid-phase dehydrogenation and can be easily separated from the reaction mixture as compared to dissolved metal complexes.

### 2.1. Monometallic Catalysts

Au bulk catalysts are inactive for the formic acid dehydrogenation. Surprisingly, Au NPs anchored on specific supports are highly active for this reaction, due to its surface electronic structure change resulting from the strong metal–support interaction. Xu et al. investigated the relationship between Au NPs and spherical SiO<sub>2</sub>, and found that Au NPs coated with amine-functionalized SiO<sub>2</sub> spheres showed high dehydrogenation rates, releasing CO-free hydrogen at 363 K [15]. Au NPs coated with SiO<sub>2</sub> spheres without amine modification possessed much poor catalytic activity. Cao et al. anchored ~1.8 nm Au NPs on the acid-resistant ZrO<sub>2</sub> by regulating the deposition and activation processes [16]. The resultant Au/ZrO<sub>2</sub> catalyst was highly active for the dehydrogenation of formic acid/triethylamine mixture, achieving an initial turnover frequency (TOF) value of 1590 h<sup>-1</sup> at 323 K, without any traces of CO. The TOF value maintained at 1200 h<sup>-1</sup> even after 100 h of continuous operation at 323 K. Zhang et al. loaded Au NPs on the Schiff base modified SiO<sub>2</sub> surface, which showed fast dehydrogenation of high concentrations of formic acid in the absence of additives, owing to the excellent C-H bond activation performance

of the interfaces between the protonated Schiff base and Au atoms [17]. The initial TOF value reached as high as  $4368 \text{ h}^{-1}$  at 323 K and the formic acid concentration of  $10 \text{ mol L}^{-1}$ .

For the gas-phase reaction over catalysts with approximately the same mean size of the Au particles (2.4–3 nm) supported on different oxide supports, Zacharska et al. also demonstrated that the hydrogen production from formic acid strongly depends on the nature of the support [18]. An Au/Al<sub>2</sub>O<sub>3</sub> catalyst showed a better performance in the reaction. The catalytic properties of this catalyst could be further improved by doping with potassium ions [19]. Recently, Bulushev et al. showed that the doping of an Au catalyst supported on carbon nanotubes with cucurbituril led to a significant decrease of the reaction temperature by 110 K due to the hydrogen abstraction from formic acid by carbonyl portals of cucurbituril [20].

Compared to Au catalysts, Pd NPs were explored extensively for the formic acid dehydrogenation. Yu et al. encapsulated ultrafine Pd NPs (~1.5 nm) inside the pores of Silicalite (MFI), which were highly active for the dehydrogenation of formic acid/sodium formate mixture, and the TOF value reached  $3027 \text{ h}^{-1}$  at 323 K with 100% hydrogen selectivity [21]. Yu et al. further found that the simultaneous encapsulation of Pd NPs and Ni(OH)<sub>2</sub> within zeolite S-1 boosted the catalytic activity of Pd NPs significantly [22]. The initial TOF value reached  $5803 \text{ h}^{-1}$  at 333 K, when the optimal molar ratio of Pd and Ni(OH)<sub>2</sub> was 4/1.

In Xu's group, a series of highly catalytically active Pd NPs were synthesized for the dehydrogenation of formic acid: (a) by using an NaOH-assisted NaBH<sub>4</sub> reduction strategy, highly dispersed Pd NPs were immobilized on porous carbon MSC-30, which possessed a TOF value of  $2623 \text{ h}^{-1}$  at 323 K and 100% hydrogen selectivity [23]; (b) by using anhydrous methanol as a surface capping agent and reducing agent, ultrafine Pd NPs (~1.4 nm) were loaded on porous carbon Vulcan XC-72R, which showed an initial TOF value of  $4452 \text{ h}^{-1}$  at 323 K [24]; (c) by functionalizing graphene oxide with *p*-phenylenediamine (PDA), highly dispersed Pd NPs (~1.5 nm) were immobilized on the surface of graphene, which showed a TOF value of  $3810 \text{ h}^{-1}$  at 323 K; even if pure formic acid was used, this catalyst maintained high catalytic activity, achieving a TOF value of  $1500 \text{ h}^{-1}$  at the same temperature [25]; (d) by functionalizing porous carbon MSC-30 with abundant N sites through the pyrolysis of urea at low-temperature, ultrafine Pd NPs (~1.4 nm) were anchored on the surface of MSC-30, which exhibited a record TOF value of  $8414 \text{ h}^{-1}$  at 333 K and there was no change in activity and selectivity after 15 cycles [26]; and (e) highly dispersed Pd NPs were immobilized on Fe-N-C support, which produced a high TOF value of  $7361 \text{ h}^{-1}$  at 323 K without any traces of CO, owing to the strong interaction between Pd and Fe-N sites [27]. Cao et al. immobilized Au, Ir, Pt, Ru, Rh, Pd and other monometallic NPs on the surface of reduced graphite oxide (rGO) for the dehydrogenation of potassium formate solution and found that only Pd NPs showed extremely high initial TOF, up to  $11,299 \text{ h}^{-1}$  at 353 K—the other particles were inactive [28]. The lattice mismatch between the Pd nanoparticles and the surface of rGO was considered to be the main reason for the enhanced catalytic activity. Cao et al. also used the strong interaction between pyridine nitrogen sites and Pd to anchor Pd NPs on the surface of N-doped carbon [29]. The obtained Pd/N-doped carbon catalyst efficiently catalyzed the dehydrogenation of additive-free formic acid at room temperature, achieving a TOF of  $5530 \text{ h}^{-1}$  without any traces of CO.

For the gas-phase reaction, Bulushev et al. prepared supported Pd catalysts with single Pd atoms using N-doped carbon [30][31] and found that single-atom Pd sites showed a TOF value three-to-four times higher than that of Pd atoms in N-free carbon-supported Pd particles and support-free Pd catalyst. Jia et al. found that doping of dispersed Pd catalysts on different supports with potassium ions leads to an increase of the TOF values by a factor of up to 33 [32]. The TOF value reached  $3600 \text{ h}^{-1}$  at 353 K for the K-doped Pd/C catalyst with a mean particle size of 3.6 nm. Bulushev and Bulusheva recently discussed the role of supported single metal atoms in the reaction and showed that they can sometimes perform better than NPs [33]. This could also be valid for some Ru or Ir immobilized complexes [34].

Notably, the non-noble metal catalysts are more promising for commercial applications owing to their cost. However, the non-noble metal catalysts often exhibit poor catalytic activity in the dehydrogenation of formic acid, as they can be etched easily by formic acid during the dehydrogenation reaction. By pyrolysis of the cobalt acetate, phenanthroline and Vulcan XC-72R mixture at high temperature, Beller et al. synthesized carbon-supported Co active sites with good resistance to acid corrosion, which possessed excellent catalytic activity and stability for the dehydrogenation of formic acid at 371 K, achieving an average  $\text{H}_2$  production rate of  $180 \text{ mL g}_{\text{cat}}^{-1} \text{ h}^{-1}$  after continuous operation for 6 days [35], owing to the highly dispersed  $\text{CoN}_x$  active centers. Furthermore, Beller et al. synthesized the N-doped carbon-supported Co single-atom catalysts (Co-N-C) through the pyrolysis of ZnCo-ZIFs at high temperature, which exhibited high activity in the catalytic hydrogen production from formic acid in propylene carbonate solvent [36], achieving an average  $\text{H}_2$  production rate of  $319.2 \text{ mL g}_{\text{cat}}^{-1} \text{ h}^{-1}$  (initial TOF= $357 \text{ h}^{-1}$ ) much higher than that of Co NPs prepared by the same process.

## 2.2. Bimetallic and Multimetallic Catalysts

Given that the intrinsic catalytic capability of metals can be enhanced through the synergistic effect of different metal elements, the bimetallic or multimetallic catalysts are a promising choice for the highly efficient dehydrogenation of formic acid. As early as in 2008, Xing et al. prepared AgPd/C and AuPd/C for the dehydrogenation of a formic acid/sodium formate mixture, which showed much higher catalytic activities than those of Ag/C, Au/C and Pd/C [37]. By introducing  $\text{CeO}_2$  as a co-catalyst, the TOF of AuPd/C was further improved, reaching  $832 \text{ h}^{-1}$  at 373 K. This group further synthesized the AuPd@Cu/C core-shell catalyst based on the weak CO adsorption characteristic of the Au surface, which showed an average  $\text{H}_2$  production rate of  $90 \text{ mL g}^{-1} \text{ min}^{-1}$  at 365 K, with a small trace of CO [38]. Tsang et al. synthesized various core-shell catalysts by depositing Pd on the surface of MNPs, such as Ag, Rh, Au, Ru and Pt, respectively [39]. Compared with the monometallic catalysts, the catalytic capabilities of the core-shell catalysts were enhanced significantly, and Ag@Pd showed a TOF value of  $252 \text{ h}^{-1}$  at 323 K, the highest activity among all the core-shell catalysts. The enhanced catalytic capability was attributed to the strong electronic interaction between core metal and shell metal. Chen et al. synthesized AuPd NPs on porous carbon by using a  $\text{Mg}^{2+}$  ion-assisted low-temperature reduction strategy, which possessed an initial TOF value of  $1120 \text{ h}^{-1}$  for the dehydrogenation of formic acid without a trace of CO [40].

The support can control the size, distribution and metal–support interaction of MNPs, and then boost their catalytic capabilities. In an early study, Xu et al. encapsulated highly dispersed AuPd NPs inside the ethylene diamine-

modified ED-MIL-101, which showed enhanced catalytic activity for the dehydrogenation of formic acid with good resistance to CO poisoning, in comparison with AuPd NPs inside MIL-101 [41]. Since then, large numbers of bimetallic NPs were reported. For example, Yan et al. synthesized AuPd and  $\text{MnO}_x$  NPs on a composite support of ZIF-8/graphene, which showed a high activity for the catalytic hydrogen production from pure formic acid, achieving an initial TOF value of  $328 \text{ h}^{-1}$  at room temperature [42]. This group further immobilized AuPd NPs ( $\sim 2.4 \text{ nm}$ ) on amine-modified N-doped graphene, which were highly active for the dehydrogenation of formic acid, achieving an initial TOF value as high as  $4445.6 \text{ h}^{-1}$  at room temperature [43]. The enhanced catalytic activity was attributed to the low adsorption capacity of Pd surface after alloying. Xu et al. immobilized AgPd NPs ( $\sim 2.5 \text{ nm}$ ) on a  $\text{ZrO}_2/\text{C}/\text{rGO}$  support, which showed a high TOF value of  $4500 \text{ h}^{-1}$  at  $323 \text{ K}$  for the dehydrogenation of the formic acid/sodium formate mixture [44].

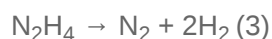
New strategies have also been developed to control the size, distribution and metal-support interaction of bimetallic NPs, and then improved their catalytic performance. Xu et al. developed a non-noble metal sacrificial approach, based on the different solubility between noble (Ag/Au/Pd) and non-noble (Co) metals in acid solution ( $\text{H}_3\text{PO}_4$ ), to immobilize highly dispersed AgPd and AuPd NPs on reduced graphene oxide (rGO), respectively [45][46]. The obtained AgPd/rGO and AuPd/rGO exhibited high activity and selectivity for the dehydrogenation of the formic acid/sodium formate mixture, achieving TOF values of  $2739 \text{ h}^{-1}$  and  $4840 \text{ h}^{-1}$  at  $323 \text{ K}$  without the releasing of CO, respectively. In addition, Xu et al. developed a solid-ligand-assisted approach, based on the strong binding ability of N sites to  $\text{Au}^{3+}$  and  $\text{Rh}^{3+}$  ions, to immobilize the bulk immiscible AuRh NPs ( $\sim 1.6 \text{ nm}$ ) on the surface of porous carbon with abundant N and O groups [47]. The pure Au or Rh NPs obtained by using the similar approach were inactive in the dehydrogenation of the formic acid/sodium formate mixture. Surprisingly, the AuRh NPs showed outstanding activity and the TOF value reached  $2297 \text{ h}^{-1}$  at  $333 \text{ K}$ .

In addition to bimetallic NPs, multimetallic NPs have exhibited much high catalytic activity and selectivity for the dehydrogenation of formic acid. Jiang et al. immobilized CoPdAu NPs and NiPdAu NPs on porous carbon Vulcan XC-72R by using a wet-chemical reduction method, respectively [48][49]. Since the second and third components modified the electronic structure of Pd, the CoPdAu/C and NiPdAu/C catalysts showed good catalytic activities, and the TOF values reached  $80$  and  $12.4 \text{ h}^{-1}$  at room temperature, respectively. Zahmakiran et al. prepared a PdNiAg/C catalyst with a particle size of  $\sim 5.6 \text{ nm}$ , which exhibited a TOF value of  $85 \text{ h}^{-1}$  at  $323 \text{ K}$  in the dehydrogenation of formic acid/sodium formate mixture [50]. Luo et al. synthesized CoAgPd NPs ( $\sim 2.8 \text{ nm}$ ) by oleic acid as a reducing agent and stabilizer [51]. Such ternary NPs achieved a TOF value of  $110 \text{ h}^{-1}$  for the dehydrogenation of the formic acid/sodium formate mixture.

### 3. Hydrazine Hydrate Dehydrogenation

Hydrazine hydrate ( $\text{N}_2\text{H}_4 \cdot \text{H}_2\text{O}$ ) is often used as a reducing agent, anti-oxidant, or fuel. Given its high hydrogen content (8.0 wt.%), outstanding thermal stability and liquid state at room temperature, hydrazine hydrate can be considered as a promising hydrogen storage material [52][53]. At the same time, this compound is toxic and it is difficult to produce hydrazine hydrate back from the by-product  $\text{N}_2$ .

If researchers use a catalyst, the hydrogen stored in hydrazine hydrate will release through two pathways: complete decomposition (3) or incomplete decomposition (4):



Complete decomposition (3) is an ideal route for producing hydrogen. Incomplete decomposition (4) produces ammonia, which not only reduces the yield of hydrogen but also poisons the fuel cell catalysts and even the environment. In order to achieve a commercial application of hydrazine hydrate as a chemical hydrogen material, the high-performance catalysts for its complete decomposition are highly desirable.

### 3.1. Monometallic Catalysts

In an earlier study, Xu et al. prepared a series of noble (Rh, Ru, Ir, Pt, Pd) and non-noble (Co, Cu, Ni, Fe) MNPs by using cetyltrimethylammonium bromide (CTAB) as a capping agent for the decomposition of hydrazine hydrate [54]. The experimental results indicated that Rh NPs have the highest hydrogen selectivity, up to 44%; Ru, Ir, Co NPs have a certain activity with the selectivity of <7%; other NPs, such as Pt, Pd, Cu, Ni, and Fe, were inactive. The researchers proposed that Ru, Ir, and Co NPs tend to break N-N bonds rather than N-H bonds, and thus promote the occurrence of incomplete decomposition. Zhang et al. prepared an Ni/Al<sub>2</sub>O<sub>3</sub> nanocatalyst by using co-precipitation method combined with high-temperature reduction and Ni-Al hydrotalcite as a raw material [55]. The Ni/Al<sub>2</sub>O<sub>3</sub> catalyst exhibited a selectivity of 93% for the complete decomposition of hydrazine hydrate at 303 K, and this selectivity was increased to 96% through the introduction of KOH. This group further used amorphous CeO<sub>2</sub> as a support to anchor Ni NPs (Ni/CeO<sub>2</sub>) [56]. When the molar ratio of Ni to CeO<sub>2</sub> was 1/0.08, the Ni/CeO<sub>2</sub> catalyst exhibited good catalytic activity (TOF = 56.1 h<sup>-1</sup>, 303 K) and selectivity (99%). Similarly, Varma et al. prepared a Ni/CeO<sub>2</sub> nanocatalyst by a solution combustion method. When the loading of Ni reached 6 wt.%, Ni/CeO<sub>2</sub> exhibited good catalytic activity (TOF = 34.0 h<sup>-1</sup>, 323 K) and H<sub>2</sub> selectivity (100%) [57].

Notably, although monometallic NPs often show poor catalytic performance for the complete decomposition of hydrazine hydrate, their catalytic performance can be improved by doping, increasing the number of basic sites and strengthening the metal–support interactions [58][59]. Wang et al. encapsulated Ni NPs inside titanate nanotubes, which exhibited a TOF value of 96.0 h<sup>-1</sup> at 333 K (1 M NaOH) and 100% H<sub>2</sub> selectivity, owing to the high dispersion of Ni NPs and the enhanced interaction between Ni and titanate [58]. Lu et al. confined Ni-CeO<sub>2</sub> nanowires on SiO<sub>2</sub> by the reverse micelle method, which possessed high catalytic activity (TOF = 219.5 h<sup>-1</sup>, 343 K) and H<sub>2</sub> selectivity (100%), due to the enhanced electronic synergistic effect between Ni NPs and the abundant oxygen vacancies of CeO<sub>2</sub> [59].

### 3.2. Bimetallic Catalysts

Compared to the studies with monometallic NPs, the studies of Ni-based alloy NPs, especially RhNi and PtNi catalysts, have contributed too much to the area of decomposition of hydrazine hydrate. In 2009, Xu et al. synthesized ~3 nm RhNi NPs by using the surface capping agent CTAB, which showed 100% H<sub>2</sub> selectivity when

the molar ratio of Rh to Ni reached 4/1 [60]. In addition, their H<sub>2</sub> selectivity relied significantly on the reaction temperature: the H<sub>2</sub> selectivity was only 28% at room temperature, however, it increased to 100% when the temperature reached 323 K [61]. In 2010, this group found that PtNi alloy NPs are highly active for the complete decomposition of hydrazine hydrate, though the Ni and Pt NPs are often inactive [62]. Since then, highly dispersed PtNi NPs (~2.4 nm) were synthesized by NaOH-assisted NaBH<sub>4</sub> reduction process, which exhibited a TOF value of 150 h<sup>-1</sup> [63]; ultrafine PtNi NPs were immobilized on 3-dimensional (3D) N-doped graphene frameworks, which achieved 100% H<sub>2</sub> selectivity and a recorded TOF value of 943 h<sup>-1</sup> at 303 K, and such 3D N-doped graphene frameworks were synthesized by the self-assembly of graphene layers with simultaneous nitrogen doping via crosslinking of graphene oxide with melamine formaldehyde resin under hydrothermal conditions followed by carbonization [64]; PtNi NPs were anchored on ZrO<sub>2</sub>/porous carbon/graphene, which showed 100% H<sub>2</sub> selectivity and a high TOF value of 1920 h<sup>-1</sup> at 323 K [65].

The strong metal–support interaction can significantly enhance the catalytic activity and selectivity of bimetallic NPs for the complete decomposition of hydrazine hydrate. In one example, Lu et al. encapsulated ultrafine PtNi NPs inside MIL-101 and found that the confinement of pores can significantly enhance the interaction between PtNi and MIL-101, thus boosting their catalytic activity (TOF = 140 h<sup>-1</sup>, 303 K), selectivity (100%) and stability (not less than 20 cycles) [66]. In another example, this group immobilized PtNi NPs on the surface of TiO<sub>2</sub>-modified Ti<sub>3</sub>C<sub>2</sub>T<sub>x</sub> nanosheets, which exhibited a high TOF value of 1220 h<sup>-1</sup> at 323 K, due to the enhanced synergistic effect between PtNi atoms and the abundant functional groups on Ti<sub>3</sub>C<sub>2</sub>T<sub>x</sub> nanosheet [67]. In addition, Wang et al. prepared N-doped carbon spheres by co-pyrolysis of SiO<sub>2</sub> spheres and dopamine for immobilizing PtNi NPs [68]. The obtained PtNi/N-doped carbon showed a high TOF value of 1602 h<sup>-1</sup> at 323 K. N-doped graphene hydrogels with abundant N sites were also used for anchoring PtNi-CeO<sub>x</sub> NPs [69]. The PtNi-CeO<sub>x</sub>/N-doped graphene hydrogels achieved a high TOF value of 3064 h<sup>-1</sup> at 323 K for the dehydrogenation of hydrazine hydrate.

PdNi and IrNi alloys are another choice for the efficient catalytic hydrogen production of hydrazine hydrate. Xu et al. found that Pd<sub>0.4</sub>Ni<sub>0.6</sub> NPs exhibited the best catalytic activity and selectivity in all their metal ratios, achieving a hydrogen selectivity of 82% at 323 K [70]. Lu et al. anchored IrNi NPs on the surface of lanthanum oxycarbonate, which showed a high TOF value of 1250 h<sup>-1</sup> at 323 K, as the abundant basic sites on the surface of lanthanum oxycarbonate facilitated the cleavage of N-H bonds [71].

In addition to Ni-based alloy, Co-based alloys also showed high catalytic performance. Yan et al. prepared Co<sub>0.65</sub>Pt<sub>0.30</sub>(CeOx)<sub>0.05</sub> nanocatalysts by a wet-chemical method, which showed H<sub>2</sub> selectivity of 72.1% at room temperature and a TOF value of 194.8 h<sup>-1</sup> [72]. Lu et al. prepared PtCo/La(OH)<sub>3</sub> catalyst, based on the outstanding synergistic effect between PtCo and the abundant basic sites on La(OH)<sub>3</sub>, which showed 100% H<sub>2</sub> selectivity and a high TOF value of 2400 h<sup>-1</sup> at 323 K [73].

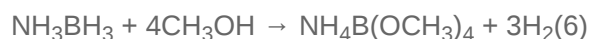
Heteroatom doping can change the electronic structure of active metals and then improve their catalytic performance. Zhang et al. introduced B element into RhNi to form a RhNiB catalyst, which possessed an eight times higher catalytic activity than that of RhNi at room temperature and alkaline conditions, and 100% H<sub>2</sub> selectivity [74]. Luo et al. synthesized graphene-supported RhNiP NPs, which showed a five times higher catalytic

activity than that of graphene-supported RhNi NPs, achieving a TOF value of  $471 \text{ h}^{-1}$  at 323 K and alkaline conditions [75]. Liu et al. prepared graphene-supported PtNiP NPs by using sodium hypophosphite as the P source [76]. Due to the synergistic effect resulting from P doping and the strong metal–graphene interaction, the  $\text{Pt}_{0.3}\text{Ni}_{0.7}\text{P}/\text{rGO}$  catalyst showed high catalytic activity for the dehydrogenation of hydrazine hydrate, demonstrating a TOF value of  $742 \text{ h}^{-1}$  at 323 K.

In order to obtain low-cost catalysts, the researchers have made great efforts to design and prepare alloy catalysts containing two non-noble elements. Lu et al. prepared  $\text{Cr}_2\text{O}_3$ -modified NiFe NPs for the dehydrogenation of hydrazine hydrate to produce hydrogen [77]. Compared to monometallic Fe and Ni catalysts, NiFe- $\text{Cr}_2\text{O}_3$  showed higher catalytic activity, and the TOF value and  $\text{H}_2$  selectivity reached  $893.5 \text{ h}^{-1}$  and 100% at 343 K, respectively. The presence of  $\text{Cr}_2\text{O}_3$  not only restricted the aggregation of NiFe NPs but also enhanced synergistic effect between NiFe and  $\text{Cr}_2\text{O}_3$ . Varma et al. prepared a NiCu/ $\text{CeO}_2$  catalyst by one-step solution combustion method for the dehydrogenation of hydrazine hydrate [78]. When the alkali concentration was 6 M and the temperature was 323 K, the TOF value reached  $1450 \text{ h}^{-1}$ —much higher than that of Ni/ $\text{CeO}_2$ . Wen et al. immobilized highly dispersed NiCo NPs (~4 nm) on the surface of ultrathin layered NiO- $\text{CoO}_x$  for the catalytic hydrogen production from hydrazine hydrate [79]. The NiCo/NiO- $\text{CoO}_x$  exhibited the TOF of  $5.49 \text{ h}^{-1}$  and 100%  $\text{H}_2$  selectivity. The interaction between metals and the high density of basic sites was considered as the main reason for its enhanced catalytic performance.

## 4. Ammonia Borane Dehydrogenation

Ammonia borane ( $\text{NH}_3\text{BH}_3$ ) is another promising chemical hydrogen storage material owing to its high hydrogen content (19.6 wt.%), low molecular weight ( $30.9 \text{ g mol}^{-1}$ ), and good solubility in water, and other solvents. Ammonia borane can release hydrogen through thermal decomposition, hydrolysis (5) or methanolysis (6) with the use of an appropriate catalyst. In the research, researchers do not consider thermal decomposition. The key to promoting the practical application of ammonia borane as hydrogen source lies in the development of efficient and stable catalysts.



For practical utilization of water solutions of ammonia borane for hydrogen production, it should be considered that it is difficult to convert the by-product  $\text{NH}_4\text{BO}_2$  back to ammonia borane due to the problems of converting the B-O bonds into the B-H bonds.

### 4.1. Hydrolysis of Ammonia Borane

#### 4.1.1. Monometallic Catalysts

In 2006, Xu et al. reported for the first time that Pt, Ru and Rh NPs possessed high catalytic activity for the hydrolysis of ammonia borane under ambient conditions [80], which attracted much attention in the scientific community on the application of ammonia borane as a practical chemical hydrogen storage material. Since then, various high-surface-area solid materials, such as porous carbon, mesoporous SiO<sub>2</sub>, metal oxides, and MOFs, have been explored as supports to anchor highly dispersed MNPs for the catalytic hydrogen production from ammonia borane. For example, a double-solvents approach was developed to encapsulate small and highly dispersed Pt NPs (~1.8 nm) inside the pores of MIL-101, which possessed high catalytic activity for the ammonia borane hydrolysis, achieving a TOF value of 414 min<sup>-1</sup> [81]. Ultrasmall and uniformly dispersed Ru NPs were immobilized on the graphene, which showed a high initial TOF value (600 min<sup>-1</sup>) at room temperature [82]. Pt and Rh NPs were immobilized on the surface of activated carbon nanotubes, which efficiently catalyzed the hydrolysis of ammonia borane to produce hydrogen, achieving high TOF values of 567 min<sup>-1</sup> and 760 min<sup>-1</sup>, respectively [83] [84]. Highly dispersed Pt NPs were anchored on the surface of graphene by a non-noble metal sacrificial approach [85], which showed a high TOF value of 284 min<sup>-1</sup> at 298 K. The MOF-derived Ru/Cu@C catalysts exhibited a TOF value of 97 min<sup>-1</sup> at room temperature for ammonia borane hydrolysis [86]. Ultrasmall Pt clusters were immobilized within the charged ionic organic molecular cage I-cage-Cl based on the electrostatic repulsion effect, and the obtained Pt@I-cage-Cl catalyst showed a unique on-off effect on the hydrolysis of ammonia borane with a TOF value of 115 min<sup>-1</sup> at 300 K [87].

Notably, non-noble metal NPs can exhibit good catalytic activity in the hydrolysis of ammonia borane, which is of great importance for practical applications. Lu et al. found that the catalytic activity of Co NPs on polyethyleneimine-modified graphene oxide was promoted by the synergistic effect of Co and amino groups, showing a TOF value of 39.9 min<sup>-1</sup> at room temperature [88]. Shaabani et al. used 3D graphene framework-supported Ni NPs to perform hydrolytic ammonia borane decomposition, and achieved a TOF value of 41.7 min<sup>-1</sup> at room temperature [89]. However, non-noble metals often show unstable catalytic activities, as they are easily oxidized in air. In this regard, the researchers synthesized CoB [90], CoP [91], and Ni<sub>2</sub>P [92] catalysts, which showed excellent anti-oxidation ability and catalytic activity in the catalytic hydrogen production from ammonia borane.

#### 4.1.2. Bimetallic Catalysts

Compared to monometallic catalysts, bimetallic catalysts often show better catalytic activity and selectivity in the hydrolysis of ammonia borane [93][94][95][96][97]. For example, Rakap et al. reported that the polyvinylpyrrolidone (PVP)-stabilized PdRh catalyst possessed a TOF value of 1333 min<sup>-1</sup> for the hydrolysis of ammonia borane at room temperature, which was much higher than that of monometallic Pd or Rh [94]. Cho et al. synthesized octahedral Au@Pt core-shell NPs by using polydiallyldimethylammonium (PDDA) as stabilizer through polyol reduction method [95]. When Pt/Au molar ratio was optimized to be 1/1, the Au@Pt nanocatalyst exhibited the best catalytic activity with an activation energy of 44.28 kJ mol<sup>-1</sup>. Yu et al. encapsulated ultrafine Rh<sub>0.8</sub>Ru<sub>0.2</sub> NPs inside Si-OH-modified MFI zeolites, which showed high catalytic activity for the hydrolysis of ammonia borane, and the TOF value reached 1006 min<sup>-1</sup> at room temperature [96].

The introduction of a non-noble metal into a noble metal catalyst can enhance the catalytic performance, while reducing the catalyst cost. Li et al. immobilized RuCu NPs (~5.4 nm) on the surface of TiO<sub>2</sub>@C-N for the hydrolysis of ammonia borane, which showed a high TOF value of 626 min<sup>-1</sup> at room temperature (based on Ru metal), when the molar ratio of Ru/Cu was 3/2 [97]. Zhang et al. immobilized Pt<sub>0.4</sub>Ni<sub>0.6</sub> NPs (~2.6 nm) on the graphene for the hydrolysis of potassium borohydride/ammonia borane mixture, which showed a TOF value of 408 min<sup>-1</sup> at 308 K [98].

By controlling the size, distribution and metal–support interaction, the catalytic performance of the bimetallic catalysts can be improved significantly. Ren et al. immobilized AuCo NPs on carbon nitride (CN) by impregnation for the catalytic hydrolysis of ammonia borane [99]. With light radiation, the AuCo/CN catalysts showed excellent catalytic activity (TOF = 2897 h<sup>-1</sup>) at room temperature. The synergistic effect between Au and Co, and the Mott–Schottky effect at the metal-semiconductor interface were responsible for the enhanced catalytic performance. By using the double-solvents approach combined with a high-concentration NaBH<sub>4</sub> reduction strategy, Xu et al. encapsulated AuNi and AuCo NPs inside the pores of MIL-101, respectively [100][101]. Owing to the small size effect and high dispersion, AuNi@MIL-101 and AuCo@MIL-101 showed catalytic activities for the hydrolysis of ammonia borane. The optimal TOF values reached 66.2 and 23.5 min<sup>-1</sup> at room temperature, respectively. Astruc et al. encapsulated ultrafine Ni<sub>2</sub>Pt NPs inside the pores of ZIF-8 by a deposition-precipitation process, which exhibited excellent catalytic activity for the hydrolysis of ammonia borane, owing to the enhanced small size effect, distribution, and metal–support interaction [102]. The optimal TOF value reached 2222 min<sup>-1</sup>. Ma et al. immobilized highly dispersed CoNi NPs on the surface of α-MoC through a strong metal–support interaction, which possessed a high catalytic activity for the hydrolysis of ammonia borane [103]. The TOF value reached 321.1 min<sup>-1</sup> at room temperature; one of the best TOF value showed by non-noble metals.

## 4.2. Methanolysis of Ammonia Borane

In recent years, researchers have explored a series of MNPs for the highly efficient methanolysis of ammonia borane, which provides a new method for the practical application of chemical hydrogen storage. In one case, Wang et al. loaded Ru NPs (~5 nm) on the surface of montmorillonite (MMT) by an ion-exchange method with hydrogen reduction, which showed an outstanding H<sub>2</sub> release rate up to 29 L min<sup>-1</sup> g<sup>-1</sup> for the methanolysis of ammonia borane [104]. Such a catalyst showed good durability, as Ru NPs were firmly stabilized inside the montmorillonite interlayers. Xu et al. used the imine molecular cage CC3R to immobilize Rh NPs, which showed excellent catalytic activity and selectivity for the methanolysis of ammonia borane, achieving a high TOF value of 215.3 min<sup>-1</sup> at room temperature [105]. The enhanced catalytic activity of Rh NPs was attributed to the good solubility of CC3 cages, which facilitated the homogenization of the heterogeneous Rh NPs with high dispersibility in reaction solvents. By N<sub>2</sub> flowing combined with water or methanol washing, the catalysts were easy to recycle after use.

Given the hydrophobicity of organic molecular cages, Xu et al. developed a reverse double-solvents approach to encapsulate ultrafine metal clusters inside the organic molecular cage RCC3 [106]. This approach involved three steps: (a) the hydrophobic RCC3 cages were dispersed into H<sub>2</sub>O solution firstly, and then a small amount of

hydrophobic solvent ( $\text{CH}_2\text{Cl}_2$ ) containing metal precursors was slowly dropped; (b) the RCC3 cages adsorbed the  $\text{CH}_2\text{Cl}_2$  containing metal precursors into their hydrophobic cavities; and (c) by reducing with the high-concentration  $\text{NaBH}_4$ , the metal precursors inside RCC3 were converted to metal clusters. The Pd@RCC3 catalyst showed a high TOF value of  $176 \text{ min}^{-1}$  at 303 K for the methanolysis of ammonia borane; one of the best activities among Pd catalysts. This group further encapsulated ultrastable Pd clusters inside the reticular Schiff base nanospaces, which showed a similar TOF value of  $177 \text{ min}^{-1}$  at 303 K for the methanolysis of ammonia borane [107]. The clean surface of metal clusters and the synergistic effect between Schiff base sites and metal atoms were responsible for the enhanced catalytic performance. In addition, Sun et al. encapsulated metal clusters inside ionic molecular cages and racemic molecular cages, which also showed excellent catalytic activities and selectivity for the catalytic methanolysis of ammonia borane [108][109].

## References

1. Majumdar, A.; Deutch, J.M.; Prasher, R.S.; Griffin, T.P. A framework for a hydrogen economy. *Joule* 2021, 5, 1905–1908.
2. Song, F.; Zhang, T.; Zhou, D.; Sun, P.; Lu, Z.; Bian, H.; Dang, J.; Gao, H.; Qian, Y.; Li, W.; et al. Charge Transfer of Interfacial Catalysts for Hydrogen Energy. *ACS Mater. Lett.* 2022, 4, 967–977.
3. Wu, C.; Li, Y.; Li, Y. *Hydrogen Storage and Transportation*; Chemical Industry Press Co., Ltd.: Beijing, China, 2020.
4. Chen, Z.; Kirlikovali, K.O.; Idrees, K.B.; Wasson, M.C.; Farha, O.K. Porous Materials for Hydrogen Storage. *Chem* 2022, 8, 693–716.
5. Onishi, N.; Laurency, G.; Beller, M.; Himeda, Y. Recent progress for reversible homogeneous catalytic hydrogen storage in formic acid and in methanol. *Coord. Chem. Rev.* 2018, 373, 317–332.
6. Lang, C.; Jia, Y.; Yao, X. Recent advances in liquid-phase chemical hydrogen storage. *Energy Storage Mater.* 2020, 26, 290–312.
7. Yang, X.; Xu, Q. Gold-containing metal nanoparticles for catalytic hydrogen generation from liquid chemical hydrides. *Chin. J. Catal.* 2016, 37, 1594–1599.
8. Onishi, N.; Iguchi, M.; Yang, X.; Kanega, R.; Kawanami, H.; Xu, Q.; Himeda, Y. Development of effective catalysts for hydrogen storage technology using formic acid. *Adv. Energy Mater.* 2019, 9, 1801275.
9. Yang, X.; Xu, Q. Encapsulating metal nanocatalysts within porous organic hosts. *Trends Chem.* 2020, 2, 214–226.

10. Wang, C.; Astruc, D. Recent developments of nanocatalyzed liquid-phase hydrogen generation. *Chem. Soc. Rev.* 2021, 50, 3437.
11. Zheng, J.; Zhou, H.; Wang, C.G.; Ye, E.; Xu, J.W.; Loh, X.J.; Li, Z. Current research progress and perspectives on liquid hydrogen rich molecules in sustainable hydrogen storage. *Energy Storage Mater.* 2021, 35, 695–722.
12. Xu, R.; Lu, W.; Toan, S.; Zhou, Z.; Russell, C.K.; Sun, Z.; Sun, Z. Thermocatalytic formic acid dehydrogenation: Recent advances and emerging trends. *J. Mater. Chem. A* 2021, 9, 24241–24260.
13. Bulushev, D.A.; Ross, J.R.H. Heterogeneous catalysts for hydrogenation of CO<sub>2</sub> and bicarbonates to formic acid and formates. *Catal. Rev.* 2018, 60, 566–593.
14. Wang, T.; Xue, W.; Wang, Y.J. Review on heterogeneous catalysts for hydrogen generation via liquid-phase formic acid decomposition. *J. Chem. Eng. Chin. Univ.* 2019, 33, 1–9.
15. Yadav, M.; Akita, T.; Tsumori, N.; Xu, Q. Strong metal–molecular support interaction (SMMSI): Amine-functionalized gold nanoparticles encapsulated in silica nanospheres highly active for catalytic decomposition of formic acid. *J. Mater. Chem.* 2012, 22, 12582–12586.
16. Bi, Q.Y.; Du, X.L.; Liu, Y.M.; Cao, Y.; He, H.Y.; Fan, K.N. Efficient subnanometric gold-catalyzed hydrogen generation via formic acid decomposition under ambient conditions. *J. Am. Chem. Soc.* 2012, 134, 8926–8933.
17. Liu, Q.Q.; Yang, X.F.; Huang, Y.Q.; Xu, S.T.; Su, X.L.; Pan, X.; Xu, J.M.; Wang, A.Q.; Liang, C.H.; Wang, X.K.; et al. A Schiff base modified gold catalyst for green and efficient H<sub>2</sub> production from formic acid. *Energy Environ. Sci.* 2015, 8, 3204.
18. Zacharska, M.; Chuvilin, A.L.; Kriventsov, V.V.; Beloshapkin, S.; Estrada, M.; Simakov, A.; Bulushev, D.A. Support effect for nanosized Au catalysts in hydrogen production from formic acid decomposition. *Catal. Sci. Technol.* 2016, 6, 6853–6860.
19. Bulushev, D.A.; Zacharska, M.; Guo, Y.; Beloshapkin, S.; Simakov, A. CO-free hydrogen production from decomposition of formic acid over Au/Al<sub>2</sub>O<sub>3</sub> catalysts doped with potassium ions. *Catal. Commun.* 2017, 92, 86–89.
20. Bulushev, D.A.; Chekhova, G.N.; Sobolev, V.I.; Chuvilin, A.L.; Fedoseeva, Y.V.; Gerasko, O.A.; Okotrub, A.V.; Bulusheva, L.G. Cucurbit uril as a co-catalyst for hydrogen production from formic acid. *Mater. Today Energy* 2022, 26, 100998.
21. Wang, N.; Sun, Q.; Bai, R.; Li, X.; Guo, G.; Yu, J. In situ confinement of ultras-small Pd clusters within nanosized silicalite-1 zeolite for highly efficient catalysis of hydrogen generation. *J. Am. Chem. Soc.* 2016, 138, 7484–7487.

22. Sun, Q.; Wang, N.; Bing, Q.; Si, R.; Liu, J.; Bai, R.; Zhang, P.; Jia, M.; Yu, J. Subnanometric hybrid Pd-M(OH)<sub>2</sub>, M = Ni, Co, clusters in zeolites as highly efficient nanocatalysts for hydrogen generation. *Chem* 2017, 3, 477–493.
23. Zhu, Q.L.; Tsumori, N.; Xu, Q. Sodium hydroxide-assisted growth of uniform Pd nanoparticles on nanoporous carbon MSC-30 for efficient and complete dehydrogenation of formic acid under ambient conditions. *Chem. Sci.* 2014, 5, 195–199.
24. Zhu, Q.L.; Tsumori, N.; Xu, Q. Immobilizing extremely catalytically active palladium nanoparticles to carbon nanospheres: A weakly-capping growth approach. *J. Am. Chem. Soc.* 2015, 137, 11743–11748.
25. Song, F.Z.; Zhu, Q.L.; Tsumori, N.; Xu, Q. Diamine-alkalized reduced graphene oxide: Immobilization of sub-2 nm palladium nanoparticles and optimization of catalytic activity for dehydrogenation of formic acid. *ACS Catal.* 2015, 5, 5141–5144.
26. Li, Z.; Yang, X.; Tsumori, N.; Liu, Z.; Himeda, Y.; Autrey, T.; Xu, Q. Tandem nitrogen functionalization of porous carbon: Toward immobilizing highly active palladium nanoclusters for dehydrogenation of formic acid. *ACS Catal.* 2017, 7, 2720–2724.
27. Zhong, S.; Yang, X.; Chen, L.; Tsumori, N.; Taguchi, N.; Xu, Q. Interfacing with Fe–N–C sites boosts the formic acid dehydrogenation of palladium nanoparticles. *ACS Appl. Mater. Interfaces* 2021, 13, 46749–46755.
28. Bi, Q.Y.; Lin, J.D.; Liu, Y.M.; Du, X.L.; Wang, J.Q.; He, H.Y.; Cao, Y. An aqueous rechargeable formate-based hydrogen battery driven by heterogenous Pd catalysis. *Angew. Chem. Int. Ed.* 2014, 53, 13583–13587.
29. Bi, Q.Y.; Lin, J.D.; Liu, Y.M.; He, H.Y.; Huang, F.Q.; Cao, Y. Dehydrogenation of formic acid at room temperature: Boosting palladium nanoparticle efficiency by coupling with pyridinic-nitrogen-doped carbon. *Angew. Chem. Int. Ed.* 2016, 55, 11849–11853.
30. Bulushev, D.A.; Zacharska, M.; Shlyakhova, E.V.; Chuvilin, A.L.; Guo, Y.; Beloshapkin, S.; Okotrub, A.V.; Bulusheva, L.G. Single isolated Pd<sup>2+</sup> cations supported on N-doped carbon as active sites for hydrogen production from formic acid decomposition. *ACS Catal.* 2016, 6, 681–691.
31. Bulushev, D.A.; Zacharska, M.; Lisitsyn, A.S.; Podyacheva, O.Y.; Hage, F.S.; Ramasse, Q.M.; Bangert, U.; Bulusheva, L.G. Single atoms of Pt-group metals stabilized by N-doped carbon nanofibers for efficient hydrogen production from formic acid. *ACS Catal.* 2016, 6, 3442–3451.
32. Jia, L.; Bulushev, D.A.; Ross, J.R.H. Formic acid decomposition over palladium-based catalysts doped by potassium carbonate. *Catal. Today* 2016, 259, 453–459.
33. Bulushev, D.A.; Bulusheva, L.G. Catalysts with single metal atoms for the hydrogen production from formic acid. *Catal. Rev.* 2021; in press.

34. Bulushev, D.A. Progress in catalytic hydrogen production from formic acid over supported metal complexes. *Energies* 2021, 14, 1334.
35. Tang, C.; Surkus, E.; Chen, F.; Pohl, M.M.; Agostini, G.; Schneider, M.; Junge, H.; Beller, M. A stable nanocobalt catalyst with highly dispersed Co<sub>Nx</sub> active sites for the selective dehydrogenation of formic acid. *Angew. Chem. Int. Ed.* 2017, 56, 16616–16620.
36. Li, X.; Surkus, A.E.; Rabeah, J.; Anwar, M.; Dastagir, S.; Junge, H.; Brückner, A.; Beller, M. Cobalt single-atom catalysts with high stability for selective dehydrogenation of formic acid. *Angew. Chem. Int. Ed.* 2020, 59, 15849–15854.
37. Zhou, X.C.; Huang, Y.J.; Xing, W.; Liu, C.P.; Liao, J.H.; Lu, T.H. High-quality hydrogen from the catalyzed decomposition of formic acid by Pd–Au/C and Pd–Ag/C. *Chem. Commun.* 2008, 30, 3540–3542.
38. Huang, Y.J.; Zhou, X.C.; Yin, M.; Liu, C.P.; Xing, W. Novel /C core–shell catalyst: Superior activity and selectivity in formic acid decomposition for hydrogen generation. *Chem. Mater.* 2010, 22, 5122–5128.
39. Tedsree, K.; Li, T.; Jones, S.; Chan, C.W.A.; Yu, K.M.K.; Bagot, P.A.J.; Marquis, E.A.; Smith, G.D.; Tsang, S.C.E. Hydrogen production from formic acid decomposition at room temperature using a Ag–Pd core–shell nanocatalyst. *Nat. Nanotechnol.* 2011, 6, 302–307.
40. Wu, S.; Yang, F.; Wang, H.; Chen, R.; Sun, P.C.; Chen, T.H. Mg<sup>2+</sup>-assisted low temperature reduction of alloyed AuPd/C: An efficient catalyst for hydrogen generation from formic acid at room temperature. *Chem. Commun.* 2015, 51, 10887–10890.
41. Gu, X.J.; Lu, Z.H.; Jiang, H.L.; Akita, T.; Xu, Q. Synergistic catalysis of metal–organic framework-immobilized Au–Pd nanoparticles in dehydrogenation of formic acid for chemical hydrogen storage. *J. Am. Chem. Soc.* 2011, 133, 11822–11825.
42. Yan, J.M.; Wang, Z.L.; Gu, L.; Li, S.J.; Wang, H.L.; Zheng, W.T.; Jiang, Q. AuPd–MnOx/MOF–graphene: An efficient catalyst for hydrogen production from formic acid at room temperature. *Adv. Energy Mater.* 2015, 5, 1500107.
43. Li, S.J.; Zhou, Y.T.; Kang, X.; Liu, D.X.; Gu, L.; Zhang, Q.H.; Yan, J.M.; Jiang, Q. A simple and effective principle for a rational design of heterogeneous catalysts for dehydrogenation of formic acid. *Adv. Mater.* 2019, 31, 1806781.
44. Song, F.Z.; Zhu, Q.L.; Yang, X.; Zhan, W.W.; Pachfule, P.; Tsumori, N.; Xu, Q. Metal-organic framework templated porous carbon-metal oxide/reduced graphene oxide as superior support of bimetallic nanoparticles for efficient hydrogen generation from formic acid. *Adv. Energy Mater.* 2018, 8, 1701416.
45. Chen, Y.; Zhu, Q.L.; Tsumori, N.; Xu, Q. Immobilizing highly catalytically active noble metal nanoparticles on reduced graphene oxide: A non-noble metal sacrificial approach. *J. Am. Chem.*

- Soc. 2015, 137, 106–109.
46. Yang, X.; Pachfule, P.; Chen, Y.; Tsumori, N.; Xu, Q. Highly efficient hydrogen generation from formic acid using a reduced graphene oxide-supported AuPd nanoparticle catalyst. *Chem. Commun.* 2016, 52, 4171–4174.
  47. Yang, X.; Li, Z.; Kitta, M.; Tsumori, N.; Guo, W.; Zhang, Z.; Zhang, J.; Zou, R.; Xu, Q. Solid-solution alloy nanoclusters of the immiscible gold-rhodium system achieved by a solid ligand-assisted approach for highly efficient catalysis. *Nano Res.* 2020, 13, 105–111.
  48. Wang, Z.L.; Yan, J.M.; Ping, Y.; Wang, H.L.; Zheng, W.T.; Jiang, Q. An efficient CoAuPd/C catalyst for hydrogen generation from formic acid at room temperature. *Angew. Chem. Int. Ed.* 2013, 52, 4406–4409.
  49. Wang, Z.L.; Ping, Y.; Yan, J.M.; Wang, H.L.; Jiang, Q. Hydrogen generation from formic acid decomposition at room temperature using a NiAuPd alloy nanocatalyst. *Int. J. Hydrog. Energy* 2014, 39, 4850–4856.
  50. Yurderi, M.; Bulut, A.; Zahmakiran, M.; Kaya, M. Carbon supported trimetallic PdNiAg nanoparticles as highly active, selective and reusable catalyst in the formic acid decomposition. *Appl. Catal. B Environ.* 2014, 160–161, 514–524.
  51. Yang, L.; Luo, W.; Cheng, G. Monodisperse CoAgPd nanoparticles assembled on graphene for efficient hydrogen generation from formic acid at room temperature. *Int. J. Hydrog. Energy* 2016, 41, 439–446.
  52. He, L.; Liang, B.; Huang, Y.; Zhang, T. Design strategies of highly selective nickel catalysts for H<sub>2</sub> production via hydrous hydrazine decomposition: A review. *Natl. Sci. Rev.* 2018, 5, 356–364.
  53. Zhang, A.; Yao, Q.; Lu, Z.H. Recent progress on catalysts for hydrogen evolution from decomposition of hydrous hydrazine. *Acta Chim. Sin.* 2021, 79, 885–902.
  54. Singh, S.K.; Zhang, X.B.; Xu, Q. Room-temperature hydrogen generation from hydrous hydrazine for chemical hydrogen storage. *J. Am. Chem. Soc.* 2009, 131, 9894–9895.
  55. He, L.; Huang, Y.; Wang, A.; Wang, X.; Chen, X.; Delgado, J.J.; Zhang, T. A noble-metal-free catalyst derived from Ni-Al hydrotalcite for hydrogen generation from N<sub>2</sub>H<sub>4</sub>·H<sub>2</sub>O decomposition. *Angew. Chem. Int. Ed.* 2012, 51, 6191–6194.
  56. He, L.; Liang, B.; Li, L.; Yang, X.; Huang, Y.; Wang, A.; Wang, X.; Zhang, T. Cerium-oxide-modified nickel as a non-noble metal catalyst for selective decomposition of hydrous hydrazine to hydrogen. *ACS Catal.* 2015, 5, 1623–1628.
  57. Kang, W.; Varma, A. Hydrogen generation from hydrous hydrazine over Ni/CeO<sub>2</sub> catalysts prepared by solution combustion synthesis. *Appl. Catal. B Environ.* 2018, 220, 409–416.

58. Wang, H.; Wu, L.; Jia, A.; Li, X.; Shi, Z.; Duan, M.; Wang, Y. Ni nanoparticles encapsulated in the channel of titanate nanotubes: Efficient noble-metal-free catalysts for selective hydrogen generation from hydrous hydrazine. *Chem. Eng. J.* 2018, 332, 637–646.
59. Huang, M.; Yao, Q.; Feng, G.; Zou, H.; Lu, Z.H. Nickel-ceria nanowires embedded in microporous silica: Controllable synthesis, formation mechanism, and catalytic applications. *Inorg. Chem.* 2020, 59, 5781–5790.
60. Singh, S.K.; Xu, Q. Complete conversion of hydrous hydrazine to hydrogen at room temperature for chemical hydrogen storage. *J. Am. Chem. Soc.* 2009, 131, 18032–18033.
61. Singh, A.K.; Yadav, M.; Aranishi, K.; Xu, Q. Temperature-induced selectivity enhancement in hydrogen generation from Rh-Ni nanoparticle-catalyzed decomposition of hydrous hydrazine. *Int. J. Hydrog. Energy* 2012, 37, 18915–18919.
62. Singh, S.K.; Xu, Q. Bimetallic Ni-Pt nanocatalysts for selective decomposition of hydrazine in aqueous solution to hydrogen at room temperature for chemical hydrogen storage. *Inorg. Chem.* 2010, 49, 6148–6152.
63. Singh, A.K.; Xu, Q. Highly-dispersed surfactant-free bimetallic Ni–Pt nanoparticles as high-performance catalyst for hydrogen generation from hydrous hydrazine. *Int. J. Hydrog. Energy* 2014, 39, 9128–9134.
64. Kumar, A.; Yang, X.; Xu, Q. Ultrafine bimetallic Pt–Ni nanoparticles immobilized on 3-dimensional N-doped graphene networks: A highly efficient catalyst for dehydrogenation of hydrous hydrazine. *J. Mater. Chem. A* 2019, 7, 112–115.
65. Song, F.Z.; Yang, X.; Xu, Q. Ultrafine bimetallic Pt–Ni nanoparticles achieved by metal-organic framework templated zirconia/porous carbon/reduced graphene oxide: Remarkable catalytic activity in dehydrogenation of hydrous hydrazine. *Small Methods* 2020, 4, 1900707.
66. Zou, H.; Zhang, S.; Hong, X.; Yao, Q.; Luo, Y.; Lu, Z.H. Immobilization of Ni-Pt nanoparticles on MIL-101/rGO composite for hydrogen evolution from hydrous hydrazine and hydrazine borane. *J. Alloys Compd.* 2020, 835, 155426.
67. Guo, F.; Zou, H.; Yao, Q.; Huang, B.; Lu, Z.H. Monodispersed bimetallic nanoparticles anchored on TiO<sub>2</sub>-decorated titanium carbide MXene for efficient hydrogen production from hydrazine in aqueous solution. *Renew. Energy* 2020, 155, 1293–1301.
68. Qiu, Y.P.; Shi, Q.; Zhou, L.L.; Chen, M.H.; Chen, C.; Tang, P.P.; Walker, G.S.; Wang, P. NiPt nanoparticles anchored onto hierarchical nanoporous N-doped carbon as an efficient catalyst for hydrogen generation from hydrazine monohydrate. *ACS Appl. Mater. Interfaces* 2020, 12, 18617–18624.
69. Du, X.; Liu, C.; Du, C.; Cai, P.; Cheng, G.; Luo, W. Nitrogen-doped graphene hydrogel-supported NiPt-CeOx nanocomposites and their superior catalysis for hydrogen generation from hydrazine

- at room temperature. *Nano Res.* 2017, 10, 2856–2865.
70. Singh, S.K.; Iizuka, Y.; Xu, Q. Nickel-palladium nanoparticle catalyzed hydrogen generation from hydrous hydrazine for chemical hydrogen storage. *Int. J. Hydrog. Energy* 2011, 36, 11794–11801.
  71. Hong, X.; Yao, Q.; Huang, M.; Du, H.; Lu, Z.H. Bimetallic NiIr nanoparticles supported on lanthanum oxy-carbonate as highly efficient catalysts for hydrogen evolution from hydrazine borane and hydrazine. *Inorg. Chem. Front.* 2019, 6, 2271–2278.
  72. Song-Il, O.; Yan, J.M.; Wang, H.L.; Wang, Z.L.; Jiang, Q. High catalytic kinetic performance of amorphous CoPt NPs induced on CeO<sub>x</sub> for H<sub>2</sub> generation from hydrous hydrazine. *Int. J. Hydrog. Energy* 2014, 39, 3755–3761.
  73. Wang, K.; Yao, Q.; Qing, S.; Lu, Z.H. La(OH)<sub>3</sub> nanosheet-supported CoPt nanoparticles: A highly efficient and magnetically recyclable catalyst for hydrogen production from hydrazine in aqueous solution. *J. Mater. Chem. A* 2019, 7, 9903–9911.
  74. Wang, J.; Li, W.; Wen, Y.; Gu, L.; Zhang, Y. Rh-Ni-B Nanoparticles as Highly Efficient Catalysts for Hydrogen Generation from Hydrous Hydrazine. *Adv. Energy Mater.* 2015, 5, 1401879.
  75. Du, X.; Tan, S.; Cai, P.; Luo, W.; Cheng, G. A RhNiP/rGO hybrid for efficient catalytic hydrogen generation from an alkaline solution of hydrazine. *J. Mater. Chem. A* 2016, 4, 14572–14576.
  76. Liu, T.; Yu, J.; Bie, H.; Hao, Z. Highly efficient hydrogen generation from hydrous hydrazine using a reduced graphene oxide-supported NiPtP nanoparticle catalyst. *J. Alloys Compd.* 2017, 690, 783–790.
  77. Chen, J.; Zou, H.; Yao, Q.; Luo, M.; Li, X.; Lu, Z.H. Cr<sub>2</sub>O<sub>3</sub>-modified NiFe nanoparticles as a noble-metal-free catalyst for complete dehydrogenation of hydrazine in aqueous solution. *Appl. Surf. Sci.* 2020, 501, 144247.
  78. Kang, W.; Guo, H.; Varma, A. Noble-metal-free NiCu/CeO<sub>2</sub> catalysts for H<sub>2</sub> generation from hydrous hydrazine. *Appl. Catal. B Environ.* 2019, 249, 54–62.
  79. Wu, D.; Wen, M.; Lin, X.; Wu, Q.; Gu, C.; Chen, H. A NiCo/NiO–CoO<sub>x</sub> ultrathin layered catalyst with strong basic sites for high-performance H<sub>2</sub> generation from hydrous hydrazine. *J. Mater. Chem. A* 2016, 4, 6595–6602.
  80. Chandra, M.; Xu, Q. A high-performance hydrogen generation system: Transition metal-catalyzed dissociation and hydrolysis of ammonia–borane. *J. Power Sources* 2006, 156, 190–194.
  81. Aijaz, A.; Karkamkar, A.; Choi, Y.J.; Tsumori, N.; Roennebro, E.; Autrey, T.; Shioyama, H.; Xu, Q. Immobilizing highly catalytically active Pt nanoparticles inside the pores of metal–organic framework: A double solvents approach. *J. Am. Chem. Soc.* 2012, 134, 13926–13929.
  82. Du, C.; Ao, Q.; Cao, N.; Yang, L.; Luo, W.; Cheng, G. Facile synthesis of monodisperse ruthenium nanoparticles supported on graphene for hydrogen generation from hydrolysis of ammonia

- borane. *Int. J. Hydrog. Energy* 2015, 40, 6180–6187.
83. Chen, W.; Ji, J.; Duan, X.; Qian, G.; Li, P.; Zhou, X.; Chen, D.; Yuan, W. Unique reactivity in Pt/CNT catalyzed hydrolytic dehydrogenation of ammonia borane. *Chem. Commun.* 2014, 50, 2142–2144.
84. Yao, Q.; Lu, Z.H.; Jia, Y.; Chen, X.; Liu, X. In situ facile synthesis of Rh nanoparticles supported on carbon nanotubes as highly active catalysts for H<sub>2</sub> generation from NH<sub>3</sub>BH<sub>3</sub> hydrolysis. *Int. J. Hydrog. Energy* 2015, 40, 2207–2215.
85. Chen, Y.; Yang, X.; Kitta, M.; Xu, Q. Monodispersed Pt nanoparticles on reduced graphene oxide by a non-noble metal sacrificial approach for hydrolytic dehydrogenation of ammonia borane. *Nano Res.* 2017, 10, 3811–3816.
86. Pachfule, P.; Yang, X.; Zhu, Q.L.; Tsumori, N.; Uchida, T.; Xu, Q. From Ru nanoparticle-encapsulated metal–organic frameworks to highly catalytically active Cu/Ru nanoparticle-embedded porous carbon. *J. Mater. Chem. A* 2017, 5, 4835–4841.
87. Zhang, S.Y.; Kochovski, Z.; Lee, H.C.; Lu, Y.; Zhang, H.; Zhang, J.; Sun, J.K.; Yuan, J. Ionic organic cage-encapsulating phase-transferable metal clusters. *Chem. Sci.* 2019, 10, 1450–1456.
88. Hu, J.; Chen, Z.; Li, M.; Zhou, X.; Lu, H. Amine-capped Co nanoparticles for highly efficient dehydrogenation of ammonia borane. *ACS Appl. Mater. Interfaces* 2014, 6, 13191–13200.
89. Mahyari, M.; Shaabani, A. Nickel nanoparticles immobilized on three-dimensional nitrogen-doped graphene as a superb catalyst for the generation of hydrogen from the hydrolysis of ammonia borane. *J. Mater. Chem. A* 2014, 2, 16652–16659.
90. Tong, D.G.; Zeng, X.L.; Chu, W.; Wang, D.; Wu, P. Magnetically recyclable hollow Co–B nanospindles as catalysts for hydrogen generation from ammonia borane. *J. Mater. Sci.* 2010, 45, 2862–2867.
91. Rakap, M. Hydrogen generation from the hydrolytic dehydrogenation of ammonia borane using electrolessly deposited cobalt–phosphorus as reusable and cost-effective catalyst. *J. Power Sources* 2014, 265, 50–56.
92. Peng, C.Y.; Kang, L.; Cao, S.; Chen, Y.; Lin, Z.S.; Fu, W.F. Nanostructured Ni<sub>2</sub>P as a robust catalyst for the hydrolytic dehydrogenation of ammonia-borane. *Angew. Chem. Int. Ed.* 2015, 54, 15725–15729.
93. Gu, J.; Yang, Y.; Tang, Y. Effects of heat-treatment on the adhesive strength of diamond films coated on the cemented carbide substrates. *J. Integr. Technol.* 2017, 6, 80–88.
94. Rakap, M. The highest catalytic activity in the hydrolysis of ammonia borane by poly(N-vinyl-2-pyrrolidone)-protected palladium–rhodium nanoparticles for hydrogen generation. *Appl. Catal. B Environ.* 2015, 163, 129–134.

95. Park, J.W.; Lai, S.W.; Cho, S.O. Catalytic hydrogen generation from hydrolysis of ammonia borane using octahedral nanoparticles. *Int. J. Hydrog. Energy* 2015, 40, 16316–16322.
96. Wang, N.; Sun, Q.; Zhang, T.; Mayoral, A.; Li, L.; Zhou, X.; Xu, J.; Zhang, P.; Yu, J. Impregnating subnanometer metallic nanocatalysts into self-pillared zeolite nanosheets. *J. Am. Chem. Soc.* 2021, 143, 6905–6914.
97. Huang, X.; Liu, Y.; Wen, H.; Shen, R.; Mehdi, S.; Wu, X.; Liang, E.; Guo, X.; Li, B. Ensemble-boosting effect of Ru-Cu alloy on catalytic activity towards hydrogen evolution in ammonia borane hydrolysis. *Appl. Catal. B Environ.* 2021, 287, 119960.
98. Guo, J.; Li, X.; Duan, H.; Zhang, H.; Jia, Q.; Zhang, S. Graphene supported Pt–Ni bimetallic nanoparticles for efficient hydrogen generation from KBH<sub>4</sub>/NH<sub>3</sub>BH<sub>3</sub> hydrolysis. *Int. J. Hydrog. Energy* 2022, 47, 11601–11610.
99. Guo, L.T.; Cai, Y.Y.; Ge, J.M.; Zhang, Y.N.; Gong, L.H.; Li, X.H.; Wang, K.X.; Ren, Q.Z.; Su, J.; Chen, J.S. Multifunctional Au– nanocatalyst for highly efficient hydrolysis of ammonia borane. *ACS Catal.* 2015, 5, 388–392.
100. Zhu, Q.L.; Li, J.; Xu, Q. Immobilizing metal nanoparticles to metal–organic frameworks with size and location control for optimizing catalytic performance. *J. Am. Chem. Soc.* 2013, 135, 10210–10213.
101. Li, J.; Zhu, Q.L.; Xu, Q. Highly active AuCo alloy nanoparticles encapsulated in the pores of metal–organic frameworks for hydrolytic dehydrogenation of ammonia borane. *Chem. Commun.* 2014, 50, 5899–5901.
102. Fu, F.; Wang, C.; Wang, Q.; Martinez-Villacorta, A.M.; Escobar, A.; Chong, H.; Wang, X.; Moya, S.; Salmon, L.; Fouquet, E.; et al. Highly selective and sharp Volcano-type synergistic Ni<sub>2</sub> hydrogen evolution from ammonia borane hydrolysis. *J. Am. Chem. Soc.* 2018, 140, 10034–10042.
103. Ge, Y.; Qin, X.; Li, A.; Deng, Y.; Lin, L.; Zhang, M.; Yu, Q.; Li, S.; Peng, M.; Xu, Y.; et al. Maximizing the synergistic effect of CoNi catalyst on  $\alpha$ -MoC for robust hydrogen production. *J. Am. Chem. Soc.* 2021, 143, 628–633.
104. Dai, H.B.; Kang, X.D.; Wang, P. Ruthenium nanoparticles immobilized in montmorillonite used as catalyst for methanolysis of ammonia borane. *Int. J. Hydrog. Energy* 2010, 35, 10317–10323.
105. Sun, J.K.; Zhan, W.W.; Akita, T.; Xu, Q. Toward homogenization of heterogeneous metal nanoparticle catalysts with enhanced catalytic performance: Soluble porous organic cage as a stabilizer and homogenizer. *J. Am. Chem. Soc.* 2015, 137, 7063–7066.
106. Yang, X.; Sun, J.K.; Kitta, M.; Pang, H.; Xu, Q. Encapsulating highly catalytically active metal nanoclusters inside porous organic cages. *Nat. Catal.* 2018, 1, 214–220.

107. Yang, X.; Chen, L.; Liu, H.; Kurihara, T.; Horike, S.; Xu, Q. Encapsulating ultrastable metal nanoparticles within reticular Schiff base nanospaces for enhanced catalytic performance. *Cell Rep. Phys. Sci.* 2021, 2, 100289.
108. Cao, W.; Zhou, J.; Kochovski, Z.; Miao, H.; Gao, Z.; Sun, J.; Yuan, J. Ionic organic cage-encapsulated metal clusters for switchable catalysis. *Cell Rep. Phys. Sci.* 2021, 2, 100546.
109. Zhu, L.; Zhang, S.; Yang, X.; Zhuang, Q.; Sun, J.K. Toward the controlled synthesis of highly dispersed metal clusters enabled by downsizing crystalline porous organic cage supports. *Small Methods* 2022, 6, 2200591.

---

Retrieved from <https://encyclopedia.pub/entry/history/show/65638>